Stiffness Control of Soft Robotic Manipulator for Minimally Invasive Surgery (MIS) Using Scale Jamming

S.M.Hadi Sadati[1(✉)], Yohan Noh[1], S. Elnaz Naghibi[2], Kaspar Althoefer[1], and Thrishantha Nanayakkara[1]

[1] Center for Robotics Research, Department of Informatics, King's College London, Strand, London WC2R 2LS, UK
{seyedmohammadhadi.sadati,yohan.noh,kaspar.althoefer, thrish.antha}@kcl.ac.uk

[2] School of Engineering and Materials Science, Queen Mary, University of London, Mile End Rd., London E1 4NS, UK
s.e.naghibi@qmul.ac.uk

Abstract. Continuum and soft robotics showed many applications in medicine from surgery to health care where their compliant nature is advantageous in minimal invasive interaction with organs. Stiffness control is necessary for challenges with soft robots such as minimalistic actuation, less invasive interaction, and precise control and sensing. This paper presents an idea of scale jamming inspired by fish and snake scales to control the stiffness of continuum manipulators by controlling the Coulomb friction force between rigid scales. A low stiffness spring is used as the backbone for a set of round curved scales to maintain an initial helix formation while two thin fishing steel wires are used to control the friction force by tensioning. The effectiveness of the design is showed for simple elongation and bending through mathematical modelling, experiments and in comparison to similar research. The model is tested to control the bending stiffness of a STIFF-FLOP continuum manipulator module designed for surgery.

Keywords: Stiffness control · Soft robot · Continuum manipulator · Layer jamming · Scale

1 Introduction

Fabrication of variable stiffness material [1] and also variable stiffness soft manipulators, mostly designed by inspiration from octopus arms [2], and wearable robots have been widely investigated recently. They have numerous applications specially in soft surgeries where their deformable structure is beneficial to improve manoeuvrability, control and sensing [3], with less invasive interactions with organs [4-6].

The idea of jamming has been used in stiffness control through increasing the friction. Granular jamming has been utilized in design of flexible manipulators [4], [5]

The original version of this chapter was revised: An incorrect version of an author's name was published. This has been corrected. The correction to this chapter is available at https://doi.org/10.1007/978-3-319-22873-0_52

H. Liu et al. (Eds.): ICIRA 2015, Part III, LNAI 9246, pp. 141–151, 2015.
DOI: 10.1007/978-3-319-22873-0_13

and also variable stiffness joints [4], [6]. As an instance, Cheng and co-workers [4] have obtained a wider stiffness range than Jiang and co-workers [5] through granular jamming for a soft manipulator. J. Santiago and co-workers [7] presented a new scaly layer jamming design with a wire driven actuation method without any pneumatic actuation which shows some improvements in smaller design possibilities. However, granular jamming apparatus is too bulky and not appropriate for wearable applications. The hysteresis loss is also inevitable in this kind of jamming. On the other hand, layer jamming, although suitable for wearable purposes, has the problem of design, fabrication and modelling because of their multilayer structure which is necessary for the manipulator to resist buckling and the long flap length which is required to achieve large deformations [8], [9].

The layer jamming design proposed by Kim et. al. recalls the bird feathers and controls normal tension due to bending to maintain the stiffness [9]. In this research, a new simpler design inspired by the role of scales in flexural stiffness of a real fish and snake skin presented [10]. Scales with jagged contact surfaces presented here are capable of stiffness control through jamming that resists the backbone coil torsion shear force with very low hysteresis (Fig. 1). Placing the scales on a helix backbone guarantees their end-face-to-face contact even in large deformations despite their small size. Here, we have used cable tension as in catheter navigation systems [11] to engage the scales and increase the friction. However, to our best knowledge, a design combining these ideas was not previously investigated for stiffening purposes in robotics. To model the scaled helical spring, the theoretical background already existing for the helical springs under eccentric loadings [12], [13] is used.

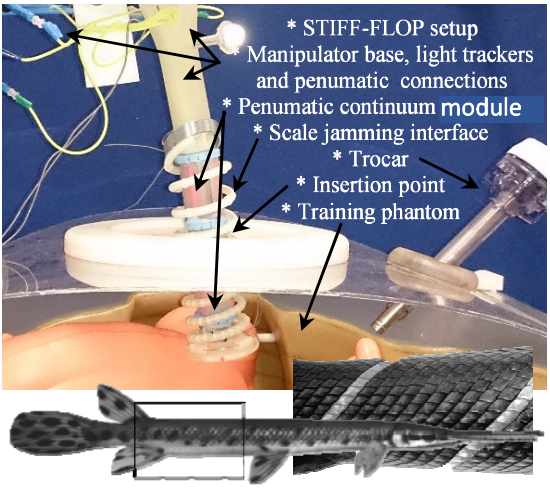

Fig. 1. STIFF-FLOP continuum manipulator with scale jamming for surgery (top), the helix like formation of scales in a fish [10] (down)

We showed that a continuum manipulator arm can be inserted in the designed scaled spring for stiffness control purposes (Fig. 1). Here, we have used a single module belonging to STIFF-FLOP manipulator, designed for surgical applications

[14], [15], inside the spring, to verify the stiffening property of the scales in bending. The module uses a set of Mckibben pneumatic actuators to achieve constant curvature bending in different directions. An alternative setup to test the proposed design in future is a tendon deriven shrinkable soft manipulator developed by F. Maghooa A. Stilli, et. al. where the manipuletor elongation is as important as its bending [16][17].

In this paper, a simple mathematical model is presented considering the elastic behaviour of the spring and the scales and LuGre friction model. The model is verified through experiments in simple elongation and bending tests. To test the bending stiffness a STIFF-FLOP module [14] is used to show the effectiveness of the idea. Finally, the advantageous of the proposed design is addressed in comparison with similar recent research.

2 Modelling

A simple piecewise static model is derived using the Castigliano's theorem to model the jammed and moving states of the scale jamming, once under external force pure tension (f_e) as in Fig. 1a-c and once under external momentum pure bending (τ_e) as in Fig. 1d, e. Spring has a rectangular cross section ($w \times h$) and the wire length (l_w), lead angle (γ) and the nominal diameter of the spring (d_s) considered to be fixed, and the lead angle changes are small and neglected. The stresses due to pure normal and shear forces are neglected since their effects are small compared to the torques effects [12]. Model parameters are presented in Table 1. The jammed scales behave similar to a rigid spring up to a breaking point related to their normal force (f_t) (elastic phase) and cause Coulomb friction damping afterwards as they move relatively (plastic phase). The scales jam again and behave like a spring if the external force reduces but the jammed state initial length (l_{c0}) should be updated during the plastic phase. The scales damping effect is modelled as a force (f_{sc}) opposing the external force and the spring deformation. The jagged surface slope angle (α) should be considered to calculate the breaking force and cancels the hysteresis at the end of a full return cycle ideally. However, a small hysteresis due to backlash between the slopes is observed and modelled by correcting the breaking force limit for the return half cycle equal to $2f_{Cb}$ where $f_{Cb} = r_{eff}.f_t.\mu_c/d_s$ is the base Coulomb friction force.

Pure Tension

For the pure tension, the spring coefficient (k_s) can be derived based on Castigliano's theorem as in [12][13] and the LuGre friction model is used to calculate the Coulomb friction torque (τ_C) due to scales' relative slip velocity (v) [18].

$$l_w = \pi d_s n_c, r_{\text{eff}} = r_i + \frac{j_{sc}}{a_{sc}}, v = \frac{2r_{\text{eff}}\,\dot{l_s}}{n_c d_s}, \tag{1}$$

$$\tau = \frac{f_e d_s}{2}, u = \int_0^{l_w} \frac{\tau^2}{2\,G\,j}\,dl_w\,, \Delta l_s = \frac{\partial u}{\partial f_e}, \tag{2}$$

$$k_{(j,G)} = f_e/\Delta l_s = 4Gj/(n_c \pi d_s^3\,), \tag{3}$$

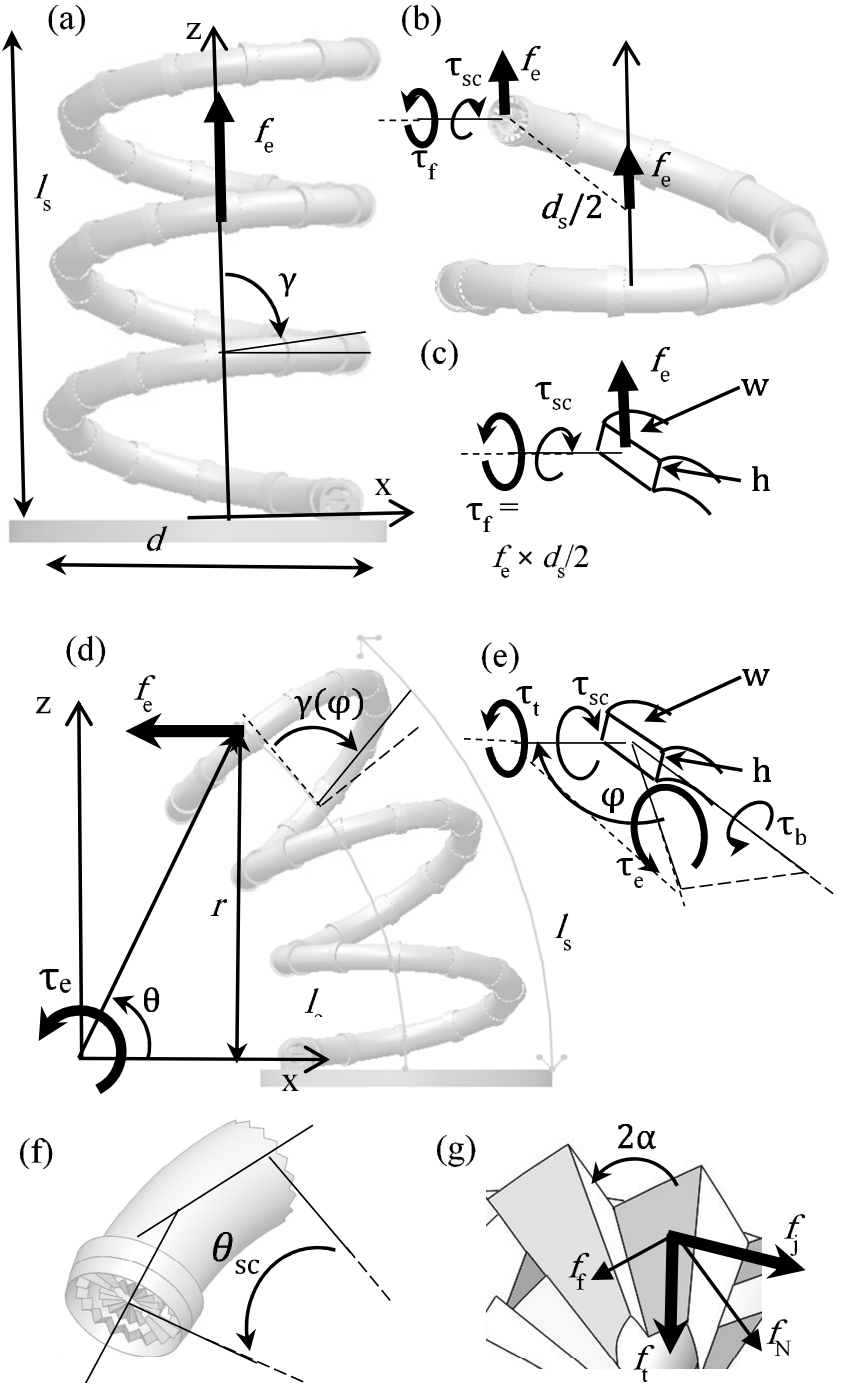

Fig. 2. Model parameters for pure tension (a-c), pure bending (d, e), and scale curvature (f) and forces on contact jagged surface (g).

$$i = f_j \sin(\alpha) - f_t \cos(\alpha) - \operatorname{sgn}(\dot{l}_s)\mu_s \left(f_j \cos(\alpha) + f_t \sin(\alpha)\right), \tag{4}$$

$$l_{c0} = \begin{cases} l_{s0} & t = 0 \\ l_{c0} & \operatorname{sgn}(i\dot{l}_s) \le 0 \ \vee \ |f_e| \le f_S - 2f_{Cb}, \\ l_s - f_{sc}/k_{(j_{sc},G_{sc})} & \text{otherwise} \end{cases} \tag{5}$$

$$C_C = \operatorname{sgn}(\dot{l}_s)(\mu_c + (\mu_s - \mu_c)e^{-(\frac{v}{v_0})^2} + \sigma_s|v|), \tag{6}$$

$$f_j = f_t\big(\cos(\alpha) + C_C \sin(\alpha)\big)/\big(\sin(\alpha) - C_C \cos(\alpha)\big), \tag{7}$$

$$f_{sc} = \begin{cases} 0 & t = 0 \\ k_{(j_{sc},G_{sc})}(l_s - l_{c0}) & \operatorname{sgn}(i\dot{l}_s) \le 0 \ \vee \ |f_e| \le f_S - 2f_{Cb}, \\ 2f_j r_{\text{eff}}/d_s & \text{otherwise} \end{cases} \tag{8}$$

$$f_s = k_{(j_s,G_s)}\Delta l_s \rightarrow \ f_e = f_{sc} + f_s, \tag{9}$$

where l_s is the spring length and $l_s^{'}$ is its deformation rate, r_{eff} is the effective radius and a_{sc} is the scale surface area, u is the strain energy due to torsional torque (τ), I is an indicator determining the slip condition, C_C is the Coulomb friction coefficient based on LuGre model, f_j and f_t are the forces acting on the jagged surface due to torsion and wire tension respectively, $f_S=2.r_{\text{eff}}.f_t.\mu_S/d_s$ is the limiting static friction, $j_s=wh(w^2+h^2)/3$ and $j_{sc}=\pi(r_o^4 - r_i^4)/4$ are the polar moment of inertia for the wire and scales.

Pure Bending

Assuming a constant curvature bending of the spring axis with constant ($l_s=l_{s0}$) under uniform external bending moment (τ_e) caused by an external force (f_e) at its end in which is similar to the case of having a constant curvature soft manipulator insides the spring. Here, θ is the spring bending angle and θ' is its time dependant rate, φ is the coil twist angle, τ_t and τ_b are the torsional and bending torques respectively, $\tau_{Cb} = r_{\text{eff}}.f_t.\mu_c$ is the base Coulomb friction torque, $\tau_S= r_{\text{eff}}.f_t.\mu_s$ is the limiting static friction torque $I_s=wh^3/12$ and $I_{sc}=\pi(r_o^4 - r_i^4)/2$ are the cross section area moment of inertia along the principal radial axis. Here the breaking occurs only in scales at $\varphi=n\pi$ positions. i and f_j are derived as in Eq.s 4 and 7.

$$r = l_{s0}/\theta, \dot{\theta} = \dot{x}_e/(r\sin(\theta)), v = -r_{\text{eff}}\dot{\theta}, \tag{10}$$

$$\tau_e = f_e r_e, \tau_t = \tau_e \cos(\phi), \tau_b = \tau_e \sin(\phi), \tag{11}$$

$$\Delta\theta = \frac{\partial u}{\partial f_e}, u_t = \int_0^{2\pi} \frac{\tau_t^2}{2\,G\,j}\frac{d_s}{2}\mathrm{d}\phi \rightarrow k_{t(j,G)} = \frac{2Gj}{n_c \pi d_s}, \tag{12}$$

$$u_b = \int_0^{2\pi} \frac{\tau_b^2}{2EI}\frac{d_s}{2}\mathrm{d}\phi \rightarrow k_{b(I,E)} = \frac{2EI}{n_c \pi d_s}, \tag{13}$$

$$\theta_{c0} = \begin{cases} \theta_0 & t = 0 \\ \theta_{c0} & \text{sgn}(i\dot{\theta}) \le 0 \ \vee \ |\tau_e| \le \tau_S - 2\tau_{Cb}, \\ \theta - \tau_{sc}/k_{t(j_{sc},G_{sc})} & \text{otherwise} \end{cases} \tag{14}$$

$$C_C = \text{sgn}(\dot{\theta})(\mu_c + (\mu_s - \mu_c)e^{-(\frac{v}{v_0})^2} + \sigma_s|v|), \tag{15}$$

$$f_{sc} = \begin{cases} 0 & t = 0 \\ k_{t(j_{sc},G_{sc})}(\theta - \theta_{c0}) & \text{sgn}(i\dot{\theta}) \le 0 \ \vee \ |\tau_e| \le \tau_S - 2\tau_{Cb}, \\ f_j r_{\text{eff}} & \text{otherwise} \end{cases} \tag{16}$$

$$\tau_s = \left(k_{t(j_s,G_s)} + k_{b(I_s,E_s)} + k_{b(I_{sc},E_{sc})}\right)\Delta\theta, \tag{17}$$

$$\rightarrow \ \tau_e = \tau_{sc} + \tau_s, \ f_e = \tau_e/r, \tag{18}$$

Table 1. Modelling Paramaters and Simulation and Experimental vaslues

E_s: Spring wire Young modulus, 60.7 [GPa]
G_s: Spring wire Shear modulus, 23.8 [GPa]
E_{sc}: Scales Young modulus for experiments, 1.28; for simulation, tension: 5.39, bending: 0.15×5.39 [GPa]
G_{sc}: Scales Shear Modulus for experiments, 0.32; for simulation, tension: 1.33, bending: 0.15×1.33 [GPa]
w: Cross section width, 1.2 [mm]
h: Cross section height, 0.2 [mm]
l_{s0}: Spring initial length in tension, 17.1 [mm]
l_{s0}: Spring initial length in torsion, 35 [mm]
d_{s0}: initial mean diameter, 38.2 [mm]
γ_0: Initial helix angle, tension: 87.3, bending: 94 [deg]
n_c: Coil turns, tension: 3, bending: 5
φ_{sc}: Scale curvature angle, 30 [deg]
n_{sc}: Number of scales, $2n_c\pi/\varphi_{sc}$
r_o: Scale end surface outer radius, 2.35 [mm]
r_i: Scale end surface inner radius, 0.8 [mm]
μ_s: Static friction coefficient, 0.03
μ_c: Coulomb friction coefficient, 0.01
v_0: Stribeck velocity, 1e-4
σ_s: Viscosity coefficient, -2e-3
r_0: Module bend curvature initial radius, for initially straight 1000, initially bent 30 [mm]
$\theta_{0:}$ Bend curvature initial angle, l_{s0}/r_0
α: Jagged surface slope angle, 50 [deg]
r_e: External force action radius in bending, 50 [mm]
σ_B: STIFF-FLOP module viscosity coefficient, -2e-2
k_B: STIFF-FLOP module stiffness constant, 33.8 [N/m]
t_f: Simulation and Experiment cycle time, 120 [s]

3 Numerical Simulation

Parameters for the numerical simulation are considered based on the experiment measurements with some modifications. A sinusoidal cyclic movement is considered as follows for l_s in tension and x_e in bending, with a=1 [cm] for tension, 7.5 [mm] for bending without initial curvature, and 5 [mm] for the bending with initial curvature.

$$l_s \text{or } x_e = a(\sin(2\pi t/t_f - \pi/2) + 1), \tag{19}$$

A simple spring-viscous damper model for the STIFF-FLOP module is considered as follows which should be added to τ_e in Eq. 18. The parameters are identified experimentally.

$$\tau_B = rk_B x_e + \sigma_B \dot{\theta}, \tag{20}$$

The simulation results for the fully jammed state show good agreement with the experimental results for the pure tension (Fig. 3), pure bending with initial curvature (Fig. 4) and bending with initial curvature (Fig.5). The simulation can predict the breaking point and hysteresis in the full cyclic actuation as well as the stiffness coefficient for the jammed and moving states with good accuracy (Fig. 3-5).

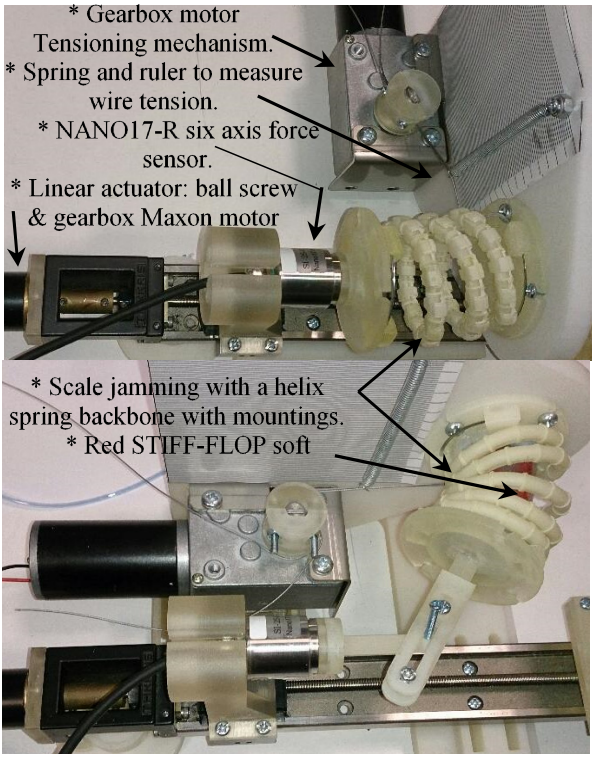

Fig. 3. Experiment setup, pure tension (up) and bending (down)

4 Experiments

A curved scale with circular cross sections is designed with a hole to pass the tension wire and 3D-printed. Both end surfaces jagged to increase the static friction while the coulomb friction is relatively low for a 3D printed part material. The experiment setup design is shown in Fig. 2 for the tension and bending experiments respectively. Fig. 3 and 4 show 40% increase in the blocking force in both tension and bending. There is a small change in stiffness constant for tension case but it is increased up to 40% in the bending test. Fig.5 shows the scales can fix the STIFF-FLOP module and block up to 0.6 [N] external force for r_0=30 [mm]. Fig. 6 shows up to 350% increase in stiffness and blocking force for antagonistic jammed state where the scales are jammed while the module chamber is pressurized which is significant. This is more than the linear summation of the system payload capacity without one of the jammed scales or internal pressure which emphasis on the antagonistic behaviour role. The results are filtered using a Moving Filter in Matlab software.

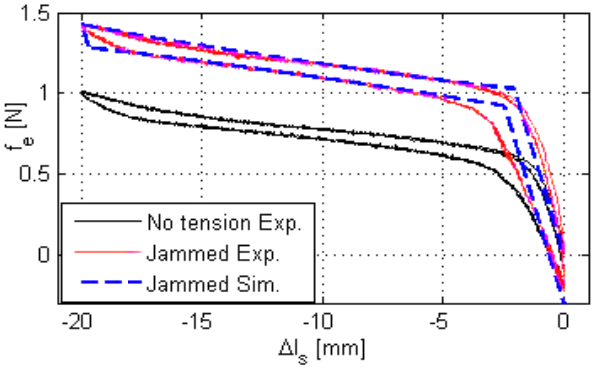

Fig. 4. Experimental and simulation results for pure tension with jammed (10N wire tension) and unjammed scales

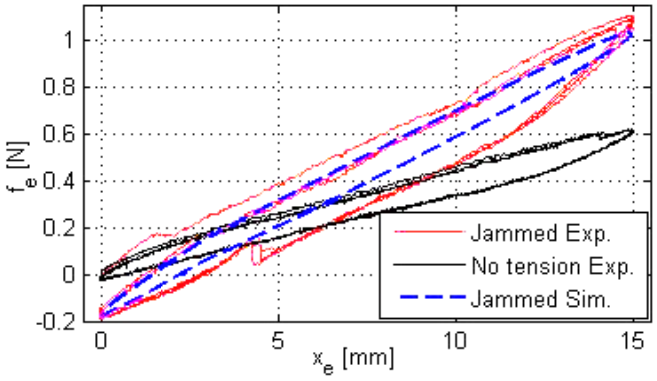

Fig. 5. Experimental and simulation results for pure bending of a straight module with jammed (1.5N wire tension) and unjammed scales

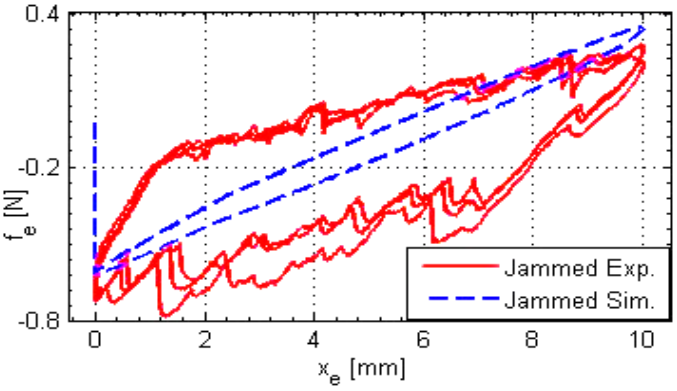

Fig. 6. Experimental and simulation results for pure bending of a bent module in jammed (1.5N wire tension) and unjammed scales

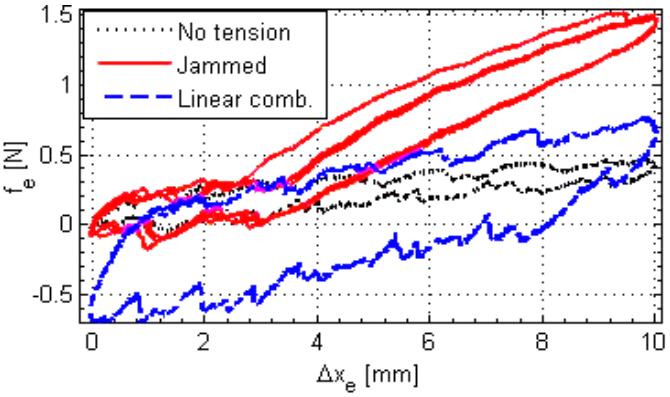

Fig. 7. Experiment results for antagonistic stiffening in pure bending for jammed (1.5N wire tension) and unjammed scales, and linear combination of scale jamming and pressurized mod-oule

5 Results and Discussion

The scale jamming in bending shows higher deformation rate ($\Delta x_e/l_{s0}$=0.428) than granular jamming by A. Jiang et. al. (=0.25) [5] and layer jamming by Kim et al. (=0.05) [9] and acts linearly in the whole deformation region while the deformation rate in the linear region for the later works are 0.18 and 0.01 respectively. The ratios of load capacity to initial length in the linear region are 28.6, 50 and 5 respectively which shows the scale jamming advantage over layer jamming. The granular jamming is better in terms of payload because of its bulky design. However, the scale jamming is better in terms of wearability, hysteresis and the ratio of achievable stiffness to device weight. The simulation results are in good agreement with the experiments; however, a more precise model considering the tensioning wire elongation and twist and the backlash between the jags is needed to achieve a model with a unified set of

parameters. Further studies on the jags shape and size as well as testing alternative tensioning mechanisms are needed to design a better implantable interface for real applications.

6 Conclusion

In this paper a new method inspired by fish scales is proposed to control the stiffness of the STIFF-FLOP continuum manipulator for surgery. The scale jamming is based on controlling the torsional shear force in a helical spring cross section with small rigid scales which reduces the weight, volume and complexity. The jagged contact surface reduces the hysteresis and increases the linear behaviour range. The results show that scale jamming provides promising opportunities for stiffness control for soft robot manipulators for minimal invasive surgery.

Acknowledgement. This research is supported by the Seventh Framework Program of the European Commission in the framework of EU project STIFF-FLOP, grant agreement 287728.

References

1. Kuder, I.K., Arrieta, A.F., Raither, W.E., Ermanni, P.: Variable stiffness material and structural concepts for morphing applications. Prog. Aerosp. Sci. **63**, 33–55 (2013)
2. Laschi, C., Cianchetti, M., Mazzolai, B., Margheri, L., Follador, M., Dario, P.: Soft Robot Arm Inspired by the Octopus. Adv. Robot. **26**(7), 709–727 (2012)
3. Sornkarn, N., Howard, M., Nanayakkara, T.: Internal Impedance Control helps Information Gain in Embodied Perception, pp. 6685–6690 (2014)
4. Cheng, N.G., Lobovsky, M.B., Keating, S.J., Setapen, A.M., Gero, K.I., Hosoi, A.E., Iagnemma, K.D.: Design and Analysis of a Robust, Low-cost, Higly Articulated Manipulator Enabled by Jamming of Granular Media, pp. 4328–4333 (2012)
5. Jiang, A., Xynogalas, G., Dasgupta, P., Althoefer, K., Nanayakkara, T.: Design of a variable stiffness flexible manipulator with composite granular jamming and membrane coupling. In: 2012 IEEE/RSJ Int. Conf. Intell. Robot. Syst., pp. 2922–2927, October 2012
6. Jiang, A., Ataollahi, A., Althoefer, K., Dasgupta, P., Nanayakkara, T.: A Variable stiffness joint by granular jamming. In: 36th Mech. Robot. Conf. Parts A B, vol. 4, p. 267, August 2012
7. Santiago, J.L.C., Walker, I.D., Godage, I.S.: Continuum robots for space applications based on layer-jamming scales with stiffening capability. In: IEEE Aerospace Conference, pp. 1–13 (2015)
8. Ou, J., Yao, L., Tauber, D., Steimle, J., Niiyama, R., Ishii, H.: JamSheets: Thin Interfaces with Tunable Stiffness Enabled by Layer Jamming (2014)
9. Kim, Y.-J., Cheng, S., Kim, S., Iagnemma, K.: A Novel Layer Jamming Mechanism With Tunable Stiffness Capability for Minimally Invasive Surgery. IEEE Trans. Robot. **29**(4), 1031–1042 (2013)
10. Long, J.H., Hale, M.E., McHenry, M.J., Westneat, M.W.: Functions of fish skin: Flexural stiffness and steady swimming of longnose gar Lepisosteus osseus. J. Exp. Biol. **199**, 2139–2151 (1996)

11. Chang, J.H., Greenlee, A.S., Cheung, K.C., Slocum, A.H., Gupta, R.: Multi-turn, tension-stiffening catheter navigation system. In: 2010 IEEE Int. Conf. Robot. Autom., pp. 5570–5575, May 2010
12. Leech, A.R.: A study of the deformation of helical springs under eccentric loading. Naval Posigraduat1e School Monterey, California (1994)
13. Michalczyk, K.: Analysis of helical compression spring support influence on its deformation. Arch. Mech. Eng., vol. LVI (2009)
14. Cianchetti, M., Ranzani, T., Gerboni, G., De Falco, I., Laschi, C., Menciassi, A.: STIFF-FLOP surgical manipulator: Mechanical design and experimental characterization of the single module. In: IEEE Int. Conf. Intell. Robot. Syst., pp. 3576–3581 (2013)
15. Cianchetti, M., Ranzani, T., Gerboni, G., Nanayakkara, T., Althoefer, K., Dasgupta, P., Menciassi, A.: Soft Robotics Technologies to Address Shortcomings in Today's Minimally Invasive Surgery: The STIFF-FLOP Approach. Soft Robot. **1**(2), 122–131 (2014)
16. Stilli, A., Wurdemann, H., Althoefer, K.: Shrinkable, stiffness-controllable soft manipulator based on a bio-inspired antagonistic actuation principle. In: IEEE/RJS International Conference on Intelligent Robots and Systems (2014)
17. Maghooa, F., Stilli, A., Althoefer, K., Wurdemann, H.: Tendon and pressure actuation for a bio-inspired manipulator based on an antagonistic principle. In: IEEE International Conference on Robotics and Automation (2015)
18. Song, X., Member, H.L., Member, K.A.: Efficient Break-Away Friction Ratio and Slip Prediction Based on Haptic Surface Exploration (2013)